

Comparative study of ion conducting pathways in borate glasses

Andreas Hall,¹ Stefan Adams,² and Jan Swenson¹

¹*Department of Applied Physics, Chalmers University of Technology, S-412 96 Göteborg, Sweden*

²*Department of Materials Science and Engineering, National University of Singapore, 117576 Singapore*

(Received 26 April 2006; published 27 November 2006)

The conduction pathways in metal-halide doped silver, lithium, and sodium diborate glasses have been examined by bond valence analysis of reverse Monte Carlo (RMC) produced structural models of the glasses. Although all glass compositions have basically the same short-range structure of the boron-oxygen network, it is evident that the intermediate-range structure is strongly dependent on the type of mobile ion. The topography of the pathways and the coordination of the pathway sites differ distinctly between the three glass systems. The mobile silver ions in the AgI-doped glass tend to be mainly iodine-coordinated and travel in homogeneously distributed pathways located in salt-rich channels of the borate network. In the NaCl-doped glass, there is an inhomogeneous spatial distribution of pathways that reflects the inhomogeneous introduction of salt ions into the glass. However, since the salt clusters are not connected, no long-range conduction pathways are formed without including also oxygen-rich regions. The pathways in the LiCl-doped glass are slightly more evenly distributed compared to the NaCl-doped glass (but not as ordered as in the AgI-doped glass), and the regions of mainly oxygen-coordinated pathway sites are of higher importance for the long-range migration. In order to more accurately investigate how these differences in the intermediate-range order of the glasses affect the ionic conductivity, we have compared the realistic structure models to more or less randomized structures. An important conclusion from this comparison is that we find no evidence that a pronounced intermediate-range order in the atomic structure or in the network of conduction pathways, as in the AgI-doped glass, is beneficial for the dc conductivity.

DOI: [10.1103/PhysRevB.74.174205](https://doi.org/10.1103/PhysRevB.74.174205)

PACS number(s): 61.43.Fs, 61.10.-i, 66.10.Ed

I. INTRODUCTION

Fast ion-conducting glasses are usually metal-halide doped glasses with ionic conductivities comparable to those in liquid electrolytes. This makes the fast ion conducting glasses attractive candidates as solid electrolytes in electrochemical devices such as solid-state microbatteries, fuel cells, chemical sensors, and “smart windows.” However, despite the increasing interest in these kinds of materials, the mechanism of the extraordinarily high ionic conductivity is still not fully understood. This is partly due to an incomplete knowledge of the microscopic structure in general and the nature of the conduction pathways for the mobile ions in particular.

In the case of the metal-halide doped oxide glasses $(MX)_x(M_2O-nA_yO_z)_{1-x}$ ($X=Cl, Br, I; A=B, P$), it is well established that the introduced dopant ions occupy interstices of the glassy structure without seriously affecting the local structure of the host glass network.¹⁻⁴ However, on an intermediate-range length scale of the order of 10 Å, it is evident from diffraction experiments and reverse Monte Carlo (RMC) modeling⁵⁻⁸ that the dopant salt AgI has a special ability to produce considerable intermediate-range ordering in the glass, manifested by the presence of an intense diffraction peak at low Q for highly AgI-doped glasses.⁹⁻¹¹ It is also these AgI-doped glasses that are the best conducting oxide glasses, with room-temperature conductivities up to 10⁻² S/cm.¹² A natural question is then, of course, whether this salt-induced intermediate-range order is an important factor for the high ionic conductivity? A first step to answer this question is to explore the origin of the intermediate-range order. For the network-forming borate and phosphate

glasses, it has been shown^{9,10} that the ordering is predominantly due to density fluctuations within the B-O or P-O network, and in none of the molecular and network glasses do correlations between the silver and iodine ions contribute substantially to the first diffraction peak in the total structure factor.¹¹ The silver ions were found to coordinate to both oxygen and iodine ions, and for the network glasses the Ag⁺ and I⁻ ions were located in pronounced pathways within the glass network. Similarly, Ag⁺ ions in crystalline phases with related compositions exhibit a mixed oxide/iodide environment.¹³

The AgI-doped glasses are often regarded as ideal model materials for investigations of the conduction mechanism in amorphous ionic conductors because of their high conductivity. However, it is the lithium- and sodium-containing glasses that appear to be the most suitable materials for technological applications due to the higher cell voltages and reduced weight of lithium batteries as well as the lower costs involved. These facts justify comprehensive studies of also the alkali-metal glasses, although their conductivities are considerably lower than those of the corresponding silver-containing glasses. In fact, in order to understand the conduction mechanism in glasses, it is crucial to find structural explanations for why the lithium- and sodium-containing glasses have lower conductivities than the corresponding silver-containing glasses, and hence to identify the crucial structural features for a high ionic conductivity. This knowledge may be useful for optimizing amorphous ionic conductors for future applications.

In the present study, we have chosen to investigate the metal-halide doped diborate glasses $(AgI)_x-(Ag_2O-2B_2O_3)_{1-x}$ ($x=0, 0.6$), $(LiCl)_x-(Li_2O-2B_2O_3)_{1-x}$ ($x=0, 0.5$),

and $(\text{NaCl})_x(\text{Na}_2\text{O}-2\text{B}_2\text{O}_3)_{1-x}$ ($x=0,0.5$) by diffraction experiments, RMC modeling, and bond valence analysis. Pure structural results from neutron and x-ray-diffraction experiments and RMC modeling have previously been published in Refs. 10 and 14. Here, we extend these studies and explore the nature of the conduction pathways in detail. We find evidence that the conduction pathways in the AgI-doped glasses are distinctly different on an intermediate-range length scale compared to the conduction pathways in LiCl- and NaCl-doped glasses. These differences are discussed in relation to the ionic conductivities of the glasses.

II. REVERSE MONTE CARLO MODELING

The RMC method has been described in detail in Refs. 6 and 7, and will therefore only be briefly introduced here. RMC uses a standard METROPOLIS Monte Carlo algorithm¹⁵ to move particles, subject to constraints, within a simulation box (Markov chain, periodic boundary conditions), but instead of minimizing the total energy, one minimizes the squared difference between the available experimental data (neutron and x-ray diffraction, extended x-ray-absorption fine structure, and nuclear magnetic resonance) and the corresponding data calculated from a computer configuration. In this way, the RMC method produces self-consistent and physically possible structures of disordered materials that agree quantitatively with (i) the available experimental input data (provided that the data do not contain significant systematic errors); (ii) certain constraints applied to ensure physically realistic configurations, e.g., closest atom-atom pair distances accepted, a connectivity between atoms in structural units or network structures in agreement with other experimental findings, and bond valence sums (see below) close to the ideal values; (iii) the experimental density of the material; and (iv) the experimental temperature.

For details of how the neutron and x-ray-diffraction experiments were performed, we refer the reader to Refs. 10 and 14. In these papers, it was also described how the RMC modeling was carried out (e.g., what kind of constraints we used for the B-O network, etc.), with the exception that our new bond-valence constraint was not included at that time. The inclusion of soft constraints on the bond-valence (cf. the next section) in the RMC modeling have also been described previously.^{16,17} In short, one can say that this constraint minimizes the deviation of the bond valence sum of each mobile ion from the respective ideal bond-valence sum in the RMC configuration without violating the agreement with the experimental data.

III. BOND-VALENCE ANALYSIS AND DETERMINATION OF PATHWAYS

The bond-valence (BV) method is essentially based on Pauling's electrostatic valence principle, which states that the sum of the electrostatic bonds reaching an ion from adjacent counterions equals the charge, Z , on that ion.¹⁸ Thereby the strength S of an individual bond in the regular coordination polyhedra of ionic compounds is determined by the ratio between its charge Z and its coordination number CN,

$$S = \frac{|Z|}{\text{CN}}. \quad (1)$$

Donnay and Allmann¹⁹ generalized this approach to a bond-length-dependent "bond valence" s_{M-X} assuming an exponential decrease of s_{M-X} with the bond length R_{M-X} ,

$$s_{M-X} = \exp\left[\frac{R_0 - R_{M-X}}{b}\right], \quad (2)$$

where the sum V_M of the individual bonds to all neighboring anions X should equal the oxidation state V_{ideal} (formal charge) of the cation M ,

$$V_M = \sum_X s_{M-X}. \quad (3)$$

This permits us to assign individual bond valences to the bonds in irregular coordination polyhedra commonly occurring in partially covalent compounds. As the values of the bond valences will be related to but not identical with bond strengths, they are usually given in "valence units" (v.u.). The parameters R_0 and b in Eq. (2) for a particular atom pair (M, X) are refined from sets of reference crystal structures. R_0 refers to the length of a bond of valence 1 v.u. (which in general is not identical to the equilibrium bond distance). b corresponds to the softness of the bond and thus how forgiving it is with deviations from the ideal bond distance. In crystal structure analysis, the bond-valence method is now routinely used to assess the plausibility of a structure determination, and the method also proved valuable in locating the positions of light atoms (such as H, Li) from x-ray-diffraction data.²⁰⁻²² In most crystals, the deviations of V from V_{ideal} , or the bond-valence mismatch $\Delta V = |V_{\text{ideal}} - V|$ for ions in their equilibrium positions, are of the order 0.05 v.u., and structures for which the root-mean-squared bond-valence sum mismatch (sometimes termed "global instability index") exceeds 0.2 are supposed to be unstable.^{23,24}

Throughout this work, we have used the parameter set from Refs. 25 and 26 for R_0 , b , and cutoff distances. Since a low value of the valence mismatch corresponds to a low site energy for an atom, it is possible to use the bond-valence approach to investigate the pathways of ionic diffusion through a structure by asserting that the bond-valence mismatch of a mobile ion should remain as low as possible.²⁴ In crystalline structures, the bond-valence mismatch thresholds that a mobile ion has to cross along its pathway in defect creation or defect migration processes in order to form an infinite ion transport pathway can be related to the respective contributions to the activation energies for ionic conduction.²⁷ Glasses behave more uniformly as the defect migration barriers usually determine the effective activation energy, but the statistical nature of the RMC structure models for glasses limits the extraction of properties from these structure models to statistical quantities. The study of individual migration barriers in a small model of a structure with large structural variations makes a determination of the lowest bond-valence mismatch corresponding to the activation energy hardly relevant. Another approach to extract transport data directly from structural models that has proven more

successful is to relate the activation energy (and conductivity) to the fraction F of the total structure volume that is occupied by the percolating pathway cluster at a fixed value of the bond-valence mismatch.^{28,29}

In order to determine the diffusion pathways of the mobile cations, the RMC produced structural model of each glass is divided into approximately 4 million cubic volume elements, each with a side length of 0.2–0.3 Å (depending on the investigated glass). Each element is marked as being accessible to an M^+ ion if it is not too close to another cation, and the bond-valence mismatch at its center is lower than a given threshold value $\Delta V \leq \Delta V_{\max}$ or if a sign change in $V_{\text{ideal}} - V$ occurs within the element. The sign-change criterion is added to avoid overlooking important connections between elements as a consequence of our limited resolution. The pathways for ac conductivity then consist of clusters of accessible sites that connect through face or edge sharing, and a percolating cluster is a pathway for dc conductivity.

In contrast to our earlier studies in which we have used the same value of ΔV_{\max} to determine the conduction pathways in different glasses, we have here instead scaled the maximum allowed bond-valence mismatch by the mass of the mobile cation as

$$\Delta V_{\max} = \Delta_0 \sqrt{m_{M^+}}, \quad (4)$$

where Δ_0 is a constant. ΔV_{\max} is expected to scale with the reduced mass of the mobile ion-anion system, but the above relation indicates that the effective anion mass may be taken as the entire glass matrix, which would result in $\mu = (m_{M^+} \cdot m_{\text{anion}} / m_{M^+} + m_{\text{anion}}) \approx m_{M^+}$. There is no precise rule for how to choose Δ_0 , but fortunately the results do not differ significantly as long as Δ_0 is not too large or too small.³⁰ A too small Δ_0 will result in a pathway structure where a majority of the volume elements of the pathway are accessible only through the sign-change criterion, resulting in an overestimation of its volume. This limit is dependent on the space resolution of the calculation and also differs from glass to glass. In the glasses examined in this work and at their resolution, this lowest possible Δ_0 value ranges from 0.014 to 0.023 v.u./u^{1/2} (valence units/atomic mass^{1/2}). If Δ_0 , on the other hand, is chosen too large, all volume elements except those occupied by immobile cations will be accessible to the mobile ion. In general, one should strive to use a Δ_0 that is close to the lowest possible value to ensure that only the most energetically favorable pathways are included in the pathway cluster. Throughout this study, we have used the value $\Delta_0 = 0.0266$ v.u./u^{1/2} corresponding to $\Delta V_{\max}(\text{Li}) = 0.07$ v.u., $\Delta V_{\max}(\text{Na}) = 0.13$ v.u. and $\Delta V_{\max}(\text{Ag}) = 0.27$ v.u.

IV. RESULTS

In our previous work, we have, as mentioned above, used a fixed value of ΔV_{\max} for a range of different glasses. The resulting volume fraction of the percolating pathway can then be related to the conductivity and activation energy by scaling it with the square root of the mobile ion mass.²⁹ In this paper, the mass scaling is performed before the volume fraction is calculated according to Eq. (4). This new scaling

of ΔV_{\max} for the investigated glasses will yield the same predictability of conductivity and activation energy as that reported earlier. In addition, since the volumes of the pathways in glasses with different types of mobile ions are now related, it is possible to compare their pathway topography to each other. A more detailed discussion of this scaling and the predictability of ionic conduction from structural RMC models will be published elsewhere.

A. Topography of pathways

Figure 1 shows 4-Å-thick slices through the percolating pathways of the six glasses in this study: $\text{Ag}_2\text{O}-2\text{B}_2\text{O}_3$, $(\text{AgI})_{0.6}-(\text{Ag}_2\text{O}-2\text{B}_2\text{O}_3)_{0.4}$, $\text{Na}_2\text{O}-2\text{B}_2\text{O}_3$, $\text{NaCl}-\text{Na}_2\text{O}-2\text{B}_2\text{O}_3$, $\text{Li}_2\text{O}-2\text{B}_2\text{O}_3$, and $\text{LiCl}-\text{Li}_2\text{O}-2\text{B}_2\text{O}_3$. All pathways are isosurfaces in the bond-valence landscape where the isovalue ΔV_{\max} for each glass is chosen in accordance with Eq. (4). Furthermore, the color of the pathways corresponds to the oxygen coordination a mobile ion would have at any given volume element in the cluster, dark gray (deep red in online copy) representing 100% oxygen coordination whereas white elements are 100% salt-anion coordinated. Some differences in the structures are striking. Looking at the undoped glasses, we see that the Ag borate has pathways similar to thick ribbons that fill the structure. The Li borate glass, on the other hand, shows much thinner pathways. The pathways of both of these glasses fill the structure in a relatively homogeneous way. A drastic difference is seen for the Na borate. Here the pathways are thicker than in the Li glass, but the distribution is highly inhomogeneous. Though we have only shown one slice through the structure for each glass, these slices are representative of the total structure of all three glasses. Turning to the doped glass structures, we see the same general tendencies as for the undoped glasses. The AgI-doped glass exhibits thick and evenly distributed pathways throughout the structure. Volume elements at the pathway surface are primarily iodine-coordinated and small regions with higher oxygen coordination act as bridges between the different saltlike regions. The LiCl-doped glass shows a higher degree of polarization in the anion coordination. Here, saltlike regions are connected through mainly oxygen-coordinated bridges that have a structure similar to the pathways in the undoped glass. Finally, the NaCl-doped glass shows an even more inhomogeneous distribution of the pathway sites than in the undoped glass. As in the LiCl-doped glass, saltlike regions connect through more oxygen-coordinated bridges, although the polarization in coordination does not seem to be as strong as for the LiCl-doped glass.

B. Oxygen coordination in conduction pathways

To further discern the distribution of coordinations to oxygens in the pathways of the three doped glasses, we determined the relative contribution from oxygen to the total bond-valence sum at each volume element in the percolating pathway, shown in Fig. 2. The AgI-doped glass shows a preference for high iodide coordination in the pathway. This effect is of course partially due to the higher dopant concentration in this glass, but it is clear that the pathway sites are

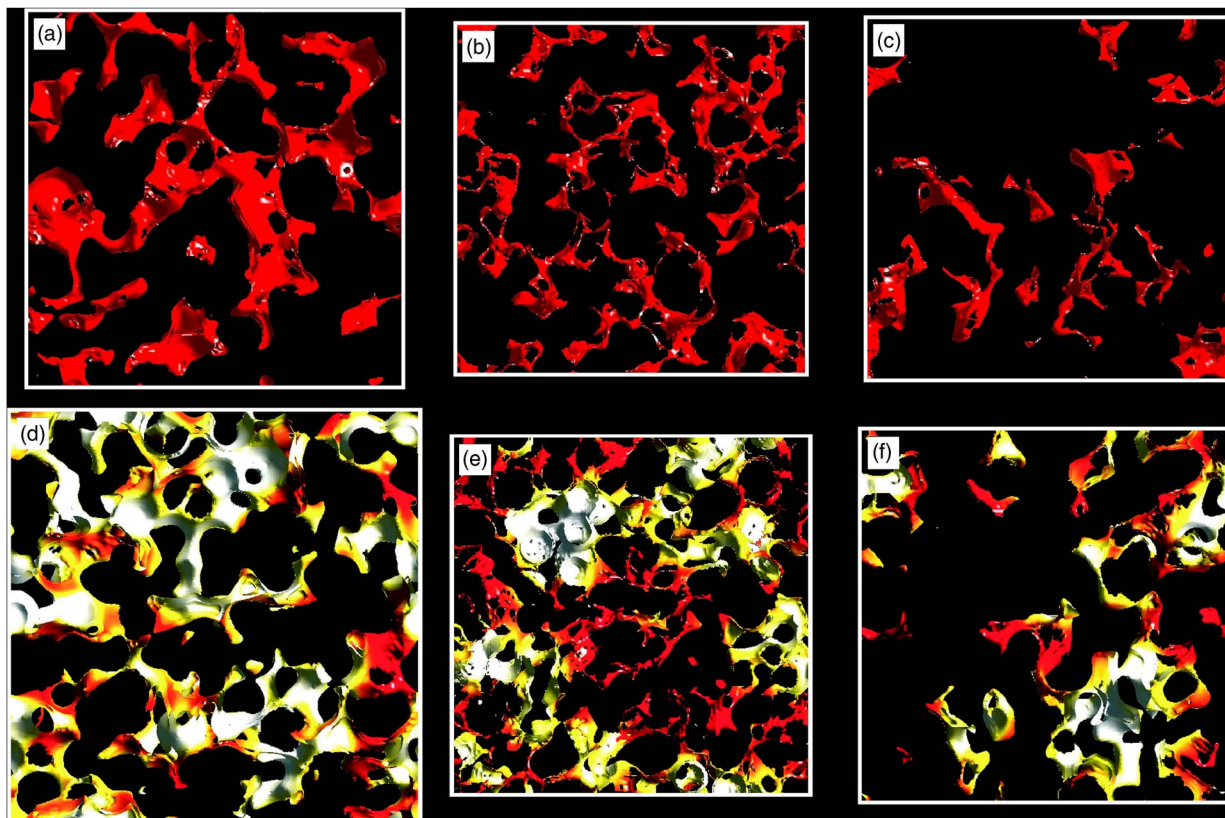


FIG. 1. (Color online) 4-Å-thick slices through the conduction pathway structures in the three undoped glasses: (a) $\text{Ag}_2\text{O}-2\text{B}_2\text{O}_3$, (b) $\text{Li}_2\text{O}-2\text{B}_2\text{O}_3$, and (c) $\text{Na}_2\text{O}-2\text{B}_2\text{O}_3$; and the three salt doped glasses (d) $(\text{AgI})_{0.6}-(\text{Ag}_2\text{O}-2\text{B}_2\text{O}_3)_{0.4}$, (e) $\text{LiCl}-\text{Li}_2\text{O}-2\text{B}_2\text{O}_3$, and (f) $\text{NaCl}-\text{Na}_2\text{O}-2\text{B}_2\text{O}_3$. The relative oxygen coordination is shown by the color where dark gray parts (red online) of the pathway have a 100% oxygen coordination, whereas fully halide coordinated parts of the pathway are white.

mainly iodine-coordinated and the number of elements with a nearly pure oxygen coordination is less than for the LiCl- and NaCl-doped glasses. The LiCl-doped glass shows a near opposite distribution to that of the AgI-doped glass. Of all glasses, it has the highest percentage of highly oxygen-coordinated volume elements. From the integrated relative frequency, shown as an inset in Fig. 2, it can be seen that 25% of all volume elements in the percolating pathway cluster have over 90% oxygen coordination. The occurrence of highly chloride-coordinated elements is, on the other hand, the lowest with only 7% of the percolating pathway volume having at least 90% chloride coordination. In the NaCl-doped glass, there is a slight preference for chloride coordination. The reason for the difference in oxygen coordination between the Li and Na pathway sites is most likely the smaller size of the Li ion, which allows it to occupy small spaces within the boron-oxygen network, where it will predominately coordinate to oxygen.

C. Pathway density correlations

To further elucidate the topographical properties of the conduction pathways, it is illustrative to use the concept of radial distribution function, commonly used to analyze diffraction data of amorphous materials. The reduced radial distribution function, $D(r)$, is defined as

$$D(r) = 4\pi r[\rho(r) - \rho_0], \quad (5)$$

where $\rho(r)$ is the pair correlation density and ρ_0 is the average pathway density. The advantage of using $D(r)$ rather than $\rho(r)$ lies directly in the amplification of small oscillations at

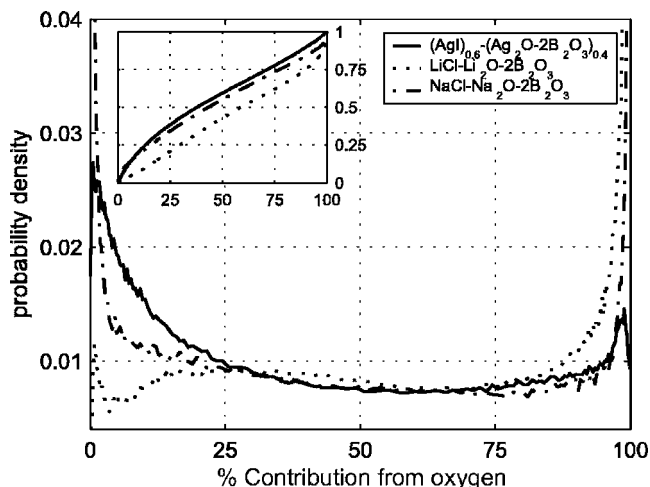


FIG. 2. Probability density of oxygen coordination in the three doped glasses. The cumulative probability (i.e., the probability that a randomly chosen site in the pathway has at most the given relative oxygen coordination) is shown as an inset.

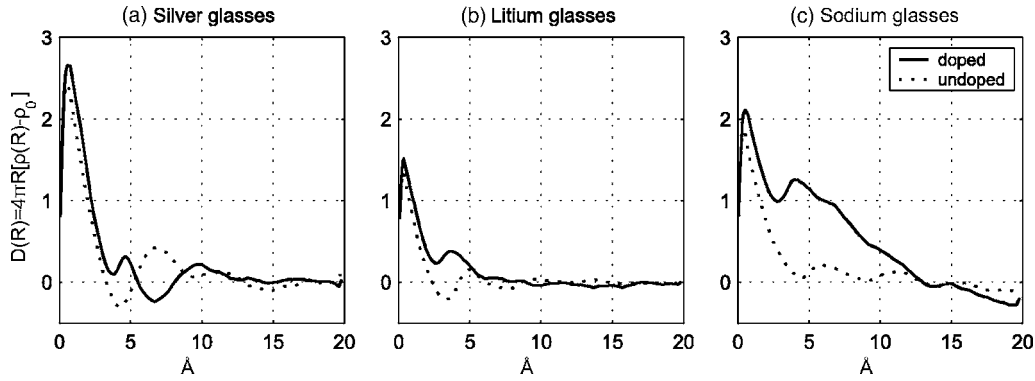


FIG. 3. Reduced radial distribution functions for the pathways in the six glasses of this study. (a) Doped and undoped Ag conducting glass, (b) doped and undoped Li conducting glass, and (c) doped and undoped Na conducting glass. The figure is redrawn from Ref. 32.

larger distances that makes identification of correlation lengths easier even though information on their relative strength becomes less intuitive. The pair correlation density was computed as the average $\rho(r)$ of 3600 volume elements, thus the positions of the volume elements included in the percolating pathway cluster correspond to the particle positions in an ordinary particle pair correlation function. Figure 3 shows $D(r)$ for the glasses studied here. The first peak that is located below 1 Å is a result of the competing increasing linear r and the decreasing $\rho(r) - \rho_0$. Its position and amplitude thus depend both on the thickness of the pathway as well as on its total volume, but do not correspond to any real pathway correlation.

All of the salt-doped glasses exhibit a peak at approximately 4 Å that is not present in the undoped glasses. This peak is caused by the halide ions that are distributed throughout the pathway cluster. Since the mobile ions cannot move arbitrarily close to the anions, there will be spheres of oversaturated positions in the pathways surrounding the embedded halide ions. Equation (2) gives that the bond length of a bond with valence s is

$$R_{M-X} = R_0 - b \ln(s_{M-X}). \quad (6)$$

In a structure as close packed as the glasses in this study it is to be expected that any pathway site would coordinate to at least two anions. Assuming that the valence is equally shared between two halide ions, we would have a maximum bond strength of $s_{M-X} = \frac{1}{2}(V_{ideal} + \Delta V_{max})$, corresponding to bond lengths of 2.3 Å in AgI, 1.8 Å in LiCl, and 2.0 Å in NaCl for the chosen values of ΔV_{max} . These radii (or rather their double value) compare well to the peak positions at 4.6, 3.5, and 3.7 Å, respectively.

The undoped Ag borate glass shows two distinct peaks in the pathway $D(r)$ above 1 Å, one at 6.6 Å and one at 11.2 Å, indicative of density fluctuations in the pathway structure on a 6–7 Å length scale, which extends to at least the second order. In the AgI-doped borate glass, there is a peak at 4.5 Å, which we earlier attributed to the existence of iodine ions embedded in the pathway, and a second broad peak at 9.7 Å. We can relate these distributions to experimental structure factors $S(Q)$ from neutron diffraction.¹⁰ The first sharp diffraction peaks (FSDP) in $S(Q)$ at 1.3 Å⁻¹ in the undoped

glass and 0.8 Å⁻¹ in the doped glass can, due to the fact that the neutron weighted $S(Q)$ for these glasses is dominated by boron and oxygen correlations, be interpreted as density fluctuations in the boron-oxygen network on length scales of 4.8 and 8 Å, respectively. The structural models obtained through RMC modeling give a vivid image (see Figs. 8 and 9 in Ref. 10) of the glass structures as borate chains separated by channels in which silver and, in the case of the doped glass, iodine ions reside. The density fluctuations of the pathway correlate fairly well to those of the glass network itself, and we see a similar expansion of the correlations upon salt doping.

The undoped Li conducting glass shows correlation peaks in the pathways at 4.9 and 9.7 Å. A previous study¹⁴ showed that the cations in this glass tend to bind to different BO_4^- groups and thus introduce void channels with a typical size of 4.6 Å between neighboring borate chain segments. These correlations in the pathway are weakened considerably when the dopant salt is introduced, leaving only a single peak at 3.5 Å, which we earlier attributed to the oversaturated volume elements surrounding the chloride ions. This loss of intermediate-range order is expected from the previous study that showed how the dopant ions are introduced inhomogeneously into the glass, creating voids in the borate structure of widely different sizes. Moreover, the pathway sites in the LiCl-doped glass are, unlike those in the AgI-doped borate, coordinating to both oxygen-rich regions as well as chloride-rich regions, which means that the pathway correlations are not expected to be similar to the structural correlations within the borate network.

The undoped Na glass exhibits weak pathway correlations at 5.8 and 11.1 Å, which can be related to the distance between two Na pathway sites separated by a borate chain, and twice this distance. The pathway correlations in the NaCl-doped glass are distinctly different compared to those in the AgI-doped glass. This glass exhibits, apart from the halide peak at 3.7 Å, a nearly featureless monotonic decrease in $D(r)$. The value of $D(r)$ is well above 0 for radii below 12 Å, which indicates a clear tendency for the pathway to cluster. As for the LiCl-doped glass, the borate network itself exhibits a loss of intermediate-range order upon introduction of the dopant salt, which explains the observed loss of pathway correlations on an intermediate-range length scale in the NaCl-doped glass.

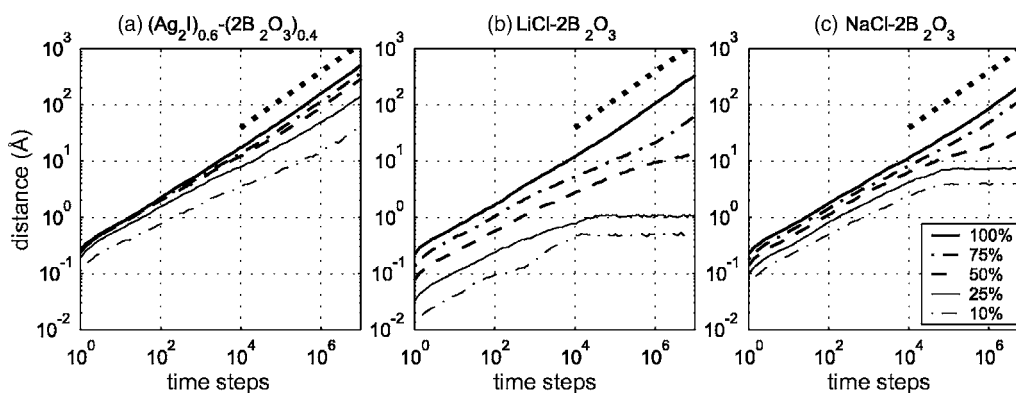


FIG. 4. Random-walk simulations of the ionic motions in the three doped glasses, where the mobile ions are restricted to only move in regions where oxygen contributes with a maximum of $X\%$ to the total bond valence ($X=100, 75, 50, 25$, and 10).

D. Random-walk simulation

As can be seen in Fig. 2, both elements with high halide coordination as well as elements with high oxygen coordination are present in the ionic pathway. To further investigate the importance of different coordinations of the mobile ions for their mobilities, it is illustrative to perform a random-walk simulation. Details of the simulation method have been presented elsewhere,¹⁶ so here we will only describe it briefly. Starting from the positions of each of the mobile ions in the RMC produced structure, in each simulation step a new position for each M^+ ion is randomly selected among its neighboring volume elements that share a face or an edge. The selected element must be accessible according to the criteria stated in Sec. III, and in addition the contribution from oxygen coordination to the total valence at the site must be below a given threshold value. Since each volume element, and thus each hop in the simulation, has a length of $0.2\text{--}0.3\text{ \AA}$, it would take an ion with thermal velocity about 10^{-13} s to cross this volume. This is of the same order as thermal vibration periods, and therefore a single hop in the simulation is not to be thought of as a jump from one equilibrium site to the next, but rather as a thermal rattling motion. Although the model is very simple and thus cannot account for all aspects of real ionic diffusion, it nevertheless gives valuable qualitative information on the structure of the pathways and the coordination of the conducting ions within the pathway clusters.

Figure 4 shows the variation of the root-mean-square (rms) displacement of the mobile ions versus pseudotime in all three doped glasses for a set of restrictions on the maximum allowed oxygen coordination. In all glasses and at all levels of restriction, the initial rms displacement follows $t^{1/2}$. This is the same as for the time evolution of a 3D random walker and thus corresponds to an unrestricted movement of the mobile ion within a local region where the pathway is three-dimensional. In all simulations, the value of the exponent drops slightly for intermediate times, indicating a restriction in the movement due to the limited local dimension of the pathways. As time increases, the slope slowly approaches $\frac{1}{2}$ again for the simulations without any restriction on oxide coordination, which is expected in an interconnected pathway structure well above the percolation limit.

While the effect of restricting the accessibility of the mobile ion to those volume elements with the highest halide coordination is qualitatively the same for all glasses, it is most pronounced in the LiCl-doped glass, due to its high content of oxygen coordination in the conduction pathway.

The Ag-doped glass [Fig. 4(a)] has the highest ionic mobility of the investigated glasses with respect to the pseudotime, and the simulation with unrestricted O coordination returns to a $t^{1/2}$ slope after roughly 10^4 time steps. Also noticeable is that the mobility does not change dramatically until a maximum of 25% oxygen coordination is allowed, and a break of percolation occurs between 25% and 10% allowed. The LiCl-doped glass [Fig. 4(b)] shows the strongest dependence of the allowed oxygen coordination on the dc conductivity. Already at the restriction of max 75% oxygen contribution, the drop in mobility is clear. The unrestricted walk reaches a $t^{1/2}$ behavior after roughly 10^5 time steps for the unrestricted walk and close to 10^7 time steps for the max 75% oxygen-coordination walk. As the maximum allowed oxygen coordination drops below 50%, the long-range diffusion is lost and the pathway is reduced to isolated clusters of accessible sites that can only contribute to ac conductivity.

Although the highly oxygen coordinated parts of the pathways are more important for the long-range diffusion in the NaCl-doped glass than in the AgI-doped glass, it does not have as strong dependence as for the LiCl-doped glass. For the unrestricted random walk a 3D-like behavior occurs after roughly 10^6 time steps. As the maximum allowed O coordination drops, the mobility decreases and at max 50% oxygen coordination the rms displacement does not reach $t^{1/2}$ behavior within the simulated time, and the transition into nonpercolating seems close. At 25% and below, we have lost the long-range diffusion and the ions are trapped in local pathway clusters.

V. DISCUSSION

From the results, it is evident that the pathways have an intermediate-range order similar to that of the borate network in all the three undoped glasses. Of the doped glasses, only AgI shows an ordering that is similar to that of the borate

network. The Ag pathways in this glass show a higher preference for halide coordination than the other doped glasses and have few volume elements that have a high degree of oxygen coordination. These findings are consistent with earlier spectroscopic studies (e.g., employing far-infrared spectroscopy),³¹ suggesting that the pathways in this glass are associated with void channels in the borate network in which the salt ions reside. In the LiCl- and NaCl-doped glasses, the pathways do not correlate in the same way to the borate network, partially due to the lack of intermediate-range order in these two glasses and partially due to the more polarized distribution of coordinations in the pathways. This is particularly the case for the LiCl-doped glass where large regions of the percolating pathway have very high oxygen coordination and thus do not reside in the salt-rich regions of the glass. The result of this fact is evident from the random-walk simulations. While the pathways in the AgI-doped glass remain percolating even if all parts that have more than 10% oxygen coordination are removed, the percolation is lost already at <50% oxygen coordination in the LiCl- and NaCl-doped glasses.

So in what way does the intermediate-range order affect the ionic conductivity in the glasses? At room temperature, the undoped Ag, Li, and Na borate glasses have ionic dc conductivities of 1.0×10^{-7} , 1.9×10^{-8} , and 2.5×10^{-10} S/cm, respectively, while the doped glasses have conductivities of 1.0×10^{-3} , 1.3×10^{-5} , and 1.0×10^{-6} S/cm (a plot of conductivity versus dopant salt concentration can be found in Ref. 32). Considering the higher dopant level in the AgI-doped glass, we have roughly the same relative increase in all three glass systems upon introduction of the dopant salt.

While the introduction of the dopant salts results in similar changes in conductivity for all three systems, the changes in intermediate-range ordering are distinctly different. In the AgI-doped glass, the length scale of the correlations in both the atomic and pathway structures increases, while the level of ordering is roughly maintained. In contrast, the intermediate order in the pathway network of the undoped lithium and sodium borate glasses is basically lost in the doped glasses, due to the inhomogeneous distribution of the salt ions in these glasses. This gives rise to two different types of pathway regions, one for salt-rich (i.e., halide-coordinated) regions and one for borate-rich (i.e., oxygen-coordinated) regions. The difference between the LiCl- and NaCl-doped glasses is then that the nature of the pathways in the borate-rich regions is very different in the two glasses, and the oxygen-coordinated regions are more extended and of higher importance for the dc conductivity in the LiCl-doped glass. Thus, these differences in how the intermediate-range structure is affected by the introduction of the dopant salt suggest that a structural ordering on an intermediate-range length scale is of subordinate importance for the dc conductivity.

A more thorough investigation of the influence of intermediate-range order on the ionic conductivity was performed by generating three types of random models of each doped glass. The first model was a hard-sphere model (HS model) where only the nearest-neighbor distances were realistic. In the second model, we included the connectivity constraints between boron and oxygen, thereby producing a proper borate network (Network model), and in the last

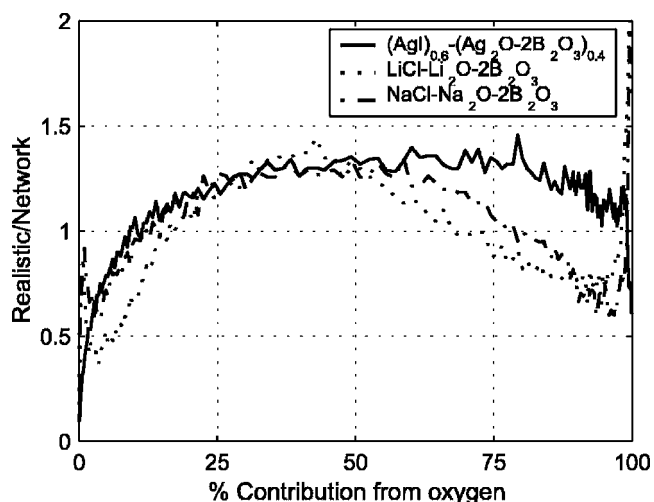


FIG. 5. Ratio between the oxygen coordination distributions of the pathways in the realistic and Network glass models of the doped glasses. The pathways of the realistic structure models show a higher probability for a mixed anion environment than the pathways in the Network models.

model we also included the bond valence constraint to ensure that the local environment of each cation is chemically reasonable (BV model). All models were generated by the RMC algorithm, but without including any experimental data. The ionic pathways in these random structures were obtained by means of bond valence computations and analyzed with the same techniques as we used for the real structures.

Another advantage with the random structures is that they give us the means to (to some extent) remove the effects of the different dopant concentrations (which were 60% for the AgI-doped glass and 50% for the NaCl- and LiCl-doped glasses), as well as the different sizes and polarizabilities of the halide ions. In this way, we can more clearly elucidate how the differences between the three glasses depend on the specific properties of the different mobile ions. Thus, Fig. 5 can be regarded as a normalized oxygen distribution of coordinations, where the effects of (i) different dopant concentrations, (ii) different anion sizes, and (iii) different anion polarizabilities have been removed. In the figure, the oxygen coordination distributions in the realistic structures of all three compositions are compared to the distributions in the Network models. In the AgI-doped glass, we can see that the realistic structure has a higher probability for sites with a mixed oxygen-halide coordination, whereas the number of sites with over 90% iodide or over 98% oxygen coordination is considerably higher in the Network model. This result is consistent with a more pronounced clustering of both salt ions and network atoms in the Network model. In the LiCl-doped glass, the Network model shows a strong drop in the number of solely oxygen-coordinated sites, but a relative increase of elements with 0–15% and 70–98% oxygen coordination, whereas the number of sites with more evenly mixed coordination drops compared to the realistic model. Thus, we see a polarization in the coordination of the pathway sites. The NaCl-doped glass shows a similar change in the coordination of the pathway sites, though the increase of

TABLE I. Volume fractions of the percolating cluster (F) and total volume fraction of the accessible elements in the four different models of each doped glass composition.

		Real	BV	Network	HS
0.6AgI	F	0.1230	0.1231	0.1200	0.0540
0.276 v.u.	Total	0.1236	0.1237	0.1202	0.0596
0.5LiCl	F	0.0608	0.0515	0.0497	0.0341
0.07 v.u.	Total	0.0612	0.0517	0.0501	0.0373
0.5NaCl	F	0.0592	0.0531	0.0485	0.0242
0.1274 v.u.	Total	0.0628	0.0534	0.0486	0.0289

highly chloride-coordinated sites is less than in the LiCl glass and we see a reduction in the number of highly oxygen-coordinated sites only for coordinations above 99%. This polarization is not due to an increased tendency for saltlike clusters, but due to changes in the structure that allow pathway volume elements with a low coordination. These elements whose valences are fulfilled mainly by one or a few anions will then to a higher degree be coordinated to a single anionic species. This larger spread of coordination numbers and oxygen contributions to the different pathway sites will cause a larger variation in the local pathway structure of the Network model.

Let us now compare the pathway volumes in the random models with those in the corresponding realistic models. Table I shows the volume of the percolating cluster as well as the total volume of accessible volume elements in the four models of each doped glass composition. The hard sphere (HS) models show the largest deviations from the realistic structures with a loss of around 50% of the pathway volumes in the latter structures. The BV and Network models, however, produce pathway volumes that are relatively close to the volumes in the realistic models. For the AgI-doped glass, the difference is less than 2% while the LiCl- and NaCl-doped glasses show a larger deviation with a relative loss of $\sim 15\%$ in the BV model and 20–25 % in the Network model. These reductions in pathway volume correspond to a decrease in conductivity with a factor 3 and 10, respectively. It is also interesting to note that the percolating pathways constitute the vast majority of the accessible volume in all models with the exception of the HS model of the NaCl-doped

glass. Thus the connectivity of the pathways seems to be reasonably stable with regard to changes in the glass structure.

The reduced pair correlation functions of the pathways in all models of the three glass compositions are shown in Fig. 6. For all glass compositions, we can see that the BV and Network models give rather similar pathway correlations. In the AgI-doped glass, the halide peak at 4.5 Å is considerably larger than that in the realistic structure. Beyond the halide peak, a weak correlation shows up at 12 Å. The increase of the halide peak and the increased correlation length from 10 to 12 Å are indications of an increased size of AgI clusters, resulting in more iodine ions residing in the middle of the pathways. In the two alkali-chloride compositions, we see instead a weakening of the halide peak as well as a small shift of it toward lower r . Beyond this peak, no composition shows any significant features in $D(r)$. The shift in the halide peak position has been interpreted to stem from the occurrence of volume elements in the pathway that have an unphysically low coordination number, thus allowing volume elements to be accessible closer to the halide ions. The BV and Network models of the NaCl-doped glass are quite similar to those of the LiCl-doped glass, with the differences being that the Na pathways are slightly thicker and the halide peak occurs at a roughly 0.5 Å higher r value, which is expected given the softer bond and larger size of the Na ion. In these two compositions, the lower halide peak indicates a reduction of the salt clusters in favor of a more homogeneous distribution of the ions.

The small change of the pathway volume in the Network and BV models of the Ag conducting glass is remarkable.

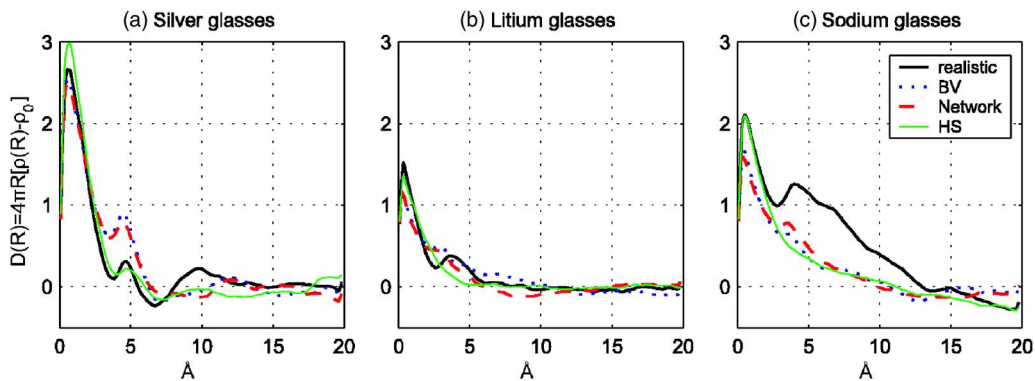


FIG. 6. (Color online) Reduced radial distribution functions of the pathway network in the realistic structure and the three random structures of each of the three doped glasses.

Although the intermediate-range order is reduced and the pathways tend to cluster more in these random structures, the pathway volume remains almost the same as we introduce a more random arrangement of the glass structure. Furthermore, the change in coordination is also relatively small, with only a shift toward more highly iodide coordinated sites in the Network and BV models. Using our bond-valence approach to predict the experimental conductivity, both the Network and the BV model of this glass would have the same conductivity as the realistic structure. This is a strong indication that the higher conductivity in the AgI-doped glass compared to the alkali halide doped glasses is predominately due to the softer bond made by the highly polarizable Ag ion to the immobile oxygen and iodine ions. Thus, the high conductivity is not a result of the pronounced intermediate-range order in this glass, although the short-range interactions are responsible also for the intermediate-range structure and the formation of pathways in the glass. This implies that a high pathway volume fraction and a high connectivity of the pathways (and possibly also the existence of salt-rich regions along which the pathways can form) in the AgI-doped glass are important for the conductivity, but that the ordering of the pathways in itself is not an important factor. The volume suitable for ionic conduction (as well as the conductivity) may then be increased by lowering the network density of the glass and thereby creating larger void regions between the borate chains where the pathways may form. The influence of the network density will hopefully be addressed in a later study on thin-film borate glasses that, through their higher cooling rate in the glass production, are expected to have a lower density than what we have in the currently investigated glass samples.

In the NaCl- and LiCl-doped glasses, the changes in pathway volume are larger as we change the structure. For the Network and BV random structures, we observed a reduction of mixed oxygen-halide coordinated sites, and more sites that are almost entirely coordinated to either a single Cl ion or a few oxygens. It is obvious that this increased number of pathway sites with an unrealistic coordination and the rapid change of coordination in the pathways are detrimental for the ionic conductivity. Thus, in these structure models the

conductivity seems to be reduced due to a less favorable local structure, again supporting our conclusion that it is mainly the local structure and the softness of the ionic bonds, rather than the degree of ordering in the intermediate-range structure of the glass or the pathway network, that determine the ionic conductivity.

VI. CONCLUDING REMARKS

We have shown that the nature of the intermediate-range order of neither the borate network nor the conduction pathways seem to affect the dc conductivity in the borate glasses studied here. Instead, it is the chemical properties, the size and softness of both the mobile ions and the halide ions, as well as the coordination of the ions in the conduction pathways, that have the highest impact on the ionic conductivity. The AgI-doped glass, which has the highest conductivity of the glasses in this study, has thick pathways with a mixed coordination that run along the walls of salt-rich channels in the glass. The reason for the thicker pathways in the Ag conducting glasses is that the bonds of the highly polarizable Ag ion to both oxygen and iodine ions are softer than the corresponding bonds in the Li and Na conducting glasses. Furthermore, in the less conducting LiCl- and NaCl-doped glasses, the pathway sites have a more polarized coordination, with parts of the pathways going through halide-rich regions connected by mainly oxygen-coordinated bridges. Although these oxygen-coordinated bridges are crucial for the long-range diffusion of the mobile ions, they are less conducting and therefore cause a reduction of the dc conductivity in these glasses.

ACKNOWLEDGMENTS

Financial support from the Hi-Condelec (NMP3-CT-2005-516975) EU STREP project, support to J.S. from the Swedish Foundation for Strategic Research, and to S.A. from the NUS Academic Research Fund (R284000029112/133) are gratefully acknowledged. J.S. is supported by a grant from the Knut and Alice Wallenberg Foundation.

¹L. Borjesson *et al.*, Phys. Rev. B **39**, 3404 (1989).

²L. Borjesson, L. M. Torell, and W. S. Howells, Philos. Mag. B **59**, 105 (1989).

³G. Carini *et al.*, Phys. Rev. B **29**, 3567 (1984).

⁴G. Chiodelli *et al.*, J. Non-Cryst. Solids **51**, 143 (1982).

⁵D. A. Keen and R. L. McGreevy, Nature (London) **344**, 423 (1990).

⁶R. L. McGreevy, Nucl. Instrum. Methods Phys. Res. A **354**, 1 (1995).

⁷R. L. McGreevy, J. Phys.: Condens. Matter **13**, 877 (2001).

⁸R. L. McGreevy, Mol. Simul. **1**, 359 (1988).

⁹J. D. Wicks *et al.*, Phys. Rev. Lett. **74**, 726 (1995).

¹⁰J. Swenson *et al.*, Phys. Rev. B **55**, 11236 (1997).

¹¹J. Swenson *et al.*, Solid State Ionics **105**, 55 (1998).

¹²A. Schiraldi *et al.*, Solid State Ionics **18-19**, 426 (1986).

¹³S. Adams, Solid State Ionics **136-137**, 1351 (2000).

¹⁴J. Swenson, L. Borjesson, and W. S. Howells, Phys. Rev. B **57**, 13514 (1998).

¹⁵N. Metropolis *et al.*, J. Chem. Phys. **21**, 1087 (1953).

¹⁶J. Swenson and S. Adams, Phys. Rev. B **64**, 024204 (2001).

¹⁷S. Adams and J. Swenson, J. Phys.: Condens. Matter **17**, 87 (2005).

¹⁸L. Pauling, J. Am. Chem. Soc. **51**, 1010 (1929).

¹⁹G. Donnay and R. Allman, Am. Mineral. **55**, 1003 (1970).

²⁰K. Waltersson, Acta Crystallogr., Sect. A: Cryst. Phys., Diffraction. Gen. Crystallogr. **A34**, 901 (1978).

²¹S. Adams, K. H. Ehses, and J. Spilker, Acta Crystallogr., Sect. B: Struct. Sci. **B49**, 958 (1993).

- ²²S. Adams, O. Moretzki, and E. Canadell, *Solid State Ionics* **168**, 281 (2004).
- ²³A. Salinas-Sanchez *et al.*, *J. Solid State Chem.* **100**, 201 (1992).
- ²⁴I. D. Brown, *The Chemical Bond in Inorganic Chemistry—The Bond Valence Model* (Oxford University Press, Oxford, 2002).
- ²⁵S. Adams, *Acta Crystallogr., Sect. B: Struct. Sci.* **B57**, 278 (2001).
- ²⁶S. Adams, <http://kristall.uni-mki.gwdg.de/softbv/>, 2004.
- ²⁷S. Adams and J. Maier, *Solid State Ionics* **105**, 67 (1998).
- ²⁸S. Adams and J. Swenson, *Phys. Rev. Lett.* **84**, 4144 (2000).
- ²⁹S. Adams and J. Swenson, *Phys. Chem. Chem. Phys.* **4**, 3179 (2002).
- ³⁰S. Adams and J. Swenson, *Phys. Rev. B* **63**, 054201 (2001).
- ³¹C. P. Varsamis, E. I. Kamitsos, and G. D. Chryssikos, *Phys. Rev. B* **60**, 3885 (1999).
- ³²A. Hall, S. Adams, and J. Swenson, *J. Non-Cryst. Solids* **352**, 5164 (2006).